Applied Computer Science 2025, vol. 21, no. 4, pp. 159–168
https://doi.org/10.35784/acs_7752

Submitted: 2025-05-16 | Revised: 2025-06-24 | Accepted: 2025-06-30

Keywords: *surface soil moisture, data fusion, residual learning, soil moisture model*

Pascal YAMAKILI [1*], *Mrindoko Rashid NICHOLAUS* [1], *Kenedy Aliila GREYSON* [2]
[1] Mbeya University of Science and Technology, Tanzania, pacoyamakilh@gmail.com, nicholausmrindoko@gmail.com
[2] Dar es Salaam Institute of Technology, Tanzania, kenedyaliila@yahoo.com
[*] Corresponding author: pacoyamakilh@gmail.com

Evaluating the impact of residual learning and feature fusion on soil moisture prediction accuracy

Abstract

The architectural design of deep learning models significantly influences their predictive capabilities in environmental monitoring tasks. This paper investigates the individual and collective effects of residual learning and feature fusion mechanism to improve the performance of soil moisture estimation on the designed architecture of the deep learning model. In this study, the data fusion mechanism was used to integrate Normalized Difference Water Index (NDWI), Synthetic Aperture Radar (SAR), and satellite imagery datasets containing Red, Green, and Blue (RGB) color channels, which consist of images or data collected by a radar system that uses microwaves to produce images of the Earth's surface. Three model variants were developed, each selectively omitting one or more of these architectural elements, and their performance was evaluated using three standard metrics, Root Mean Squared Error (RMSE), Mean Absolute Error (MAE), and Coefficient of Determination (R2). The results of the final proposed model architecture showed that while each component contributes to accuracy improvements, the combination of residual learning and feature fusion yields the most significant gains. Improved results of RMSE = 0.0117, R^2=0.814 and Mean Absolute Error =0.0148 were obtained. These performance indicators were superior to the results of most of the baseline models after comparative analysis. Thus, this study provides insights into model component selection for deep learning soil moisture prediction applications.

1. INTRODUCTION

Spatial measurement of soil moisture distribution is an important task in agriculture, hydrology, land management and climate. It always provides vital information for irrigation management, prediction of drought or flood conditions, optimization of crop yields, understanding of environmental impacts, and effective management of water resources, making it an essential tool for agriculture, environmental monitoring, and disaster preparedness (Adab et al., 2020).

Surface soil moisture measurement methods vary from those that measure the water content of the surface soil at a specific point using buried moisture sensors to remote sensing methods that use airborne methods (Brocca et al., 2010). Measuring moisture using buried sensors in an agricultural area provides moisture information on specific surface soil portions where it is difficult to infer the accurate average surface moisture over a large area with different surface soil characteristics (Famiglietti et al., 2008). Several researchers have demonstrated that when surface soil moisture measurements are made on the same piece of land under the same environmental conditions using buried sensors, there is a noticeable variability in soil moisture that generally increases with scale. Hunduma & Kebede (2020) suggested that for a scale of 2.5 m to 50 km, the moisture variation ranges from 0.036 cm^3 /cm^3 to 0.071 cm^3 /cm^3. Similarly, surface soil moisture values will always be more similar if the measurement points are close together rather than far apart. Obviously, soils of similar type and characteristics will produce little variation for closer point-to-point and soil-sampling measurements. However, there is also a need to investigate the accuracy of measurements for spatial distribution of soil moisture over large areas with similar soil type and characteristics. It is true that remote sensing technologies offer the potential for spatially continuous and temporally frequent soil moisture monitoring over large areas. However, retrieving accurate soil moisture information from satellite data remains challenging due to several factors such as Complex relationships that the relationship between satellite observations and soil moisture is non-linear and depends on multiple factors including vegetation cover, soil

texture, and surface roughness (Mohanty & Skaggs, 2001). Limited penetration depth is also a factor; most satellite sensors can only detect moisture in the top few centimeters of soil, while many applications require information about the root zone (Scott et al., 2003). The other factor is mixed pixel effects: The spatial resolution of satellite data often results in pixels containing multiple land cover types, making it difficult to extract soil-specific information (Babaeian et al., 2019). In addition, instrumental noise and atmospheric effects are among the limiting factors in remote sensing soil moisture studies. Satellite measurements are subject to various sources of noise and require careful calibration and preprocessing (Massari et al., 2017).

On the other hand, various scientists have tried to develop soil measurement methods that accurately predict average moisture values over large areas of soil. Similarly, the use of airborne methods that use satellites to map images obtained at higher altitudes to moisture values has previously been proposed (Rodriguez-Alvarez et al., 2023). However, the airborne methods the effects of mapping images captured and obtained from high altitudes from the land surface soil, reducing the accuracy of moisture estimation due to fewer image pixels considered.To overcome this, some scholars have successfully developed deep learning model using either data fusion but a combination of both data fusion and residual learning (Batchu, 2022).

Nevertheless, accurate soil moisture estimation is crucial for agricultural management and hydrological modeling, regardless of the method used. Therefore, this paper presents an innovative and accuracy improved deep learning algorithm model with the combination of residual learning and feature fusion that yields the most significant gains in terms of performance. The study introduces a novel architecture that integrates residual connections for improved soil moisture estimation from multi-source satellite data. A comprehensive ablation study was also conducted to analyze the impact of different architectural components (residual connections and feature fusion) on model performance. The study uses a benchmarking approach against state of the art models, whose observation has shown that the final model has superior performance in terms of accuracy and computational efficiency. Furthermore, the robustness of the model over different soil conditions (sandy soil, clay soil, vegetated areas, and bare soil) was evaluated, providing insight into its operational capabilities. The study also provides insights into building a forecasting application model for effective remote sensing soil moisture prediction to address the spatial soil moisture distribution using satellite imagery.

2. METHODS

2.1. Data collection and preprocessing

In this study, the dataset included images from both the Sentinel-1 and Sentinel-2 satellites. Synthetic Aperture Radar (SAR) images were collected from Sentinel-1 (satellites 1A and 1B) in two polarization modes: SAR_VV (vertical transmit and vertical receive) and SAR_VH (vertical transmit and horizontal receive). Sentinel-2 (satellites 2A and 2B) optical RGB and Normalized Difference Vegetation Index (NDVI) images were acquired. Data were processed using the near-infrared (band 8) and red (band 4) spectral bands.

Sentinel-1 provides dual-polarization C-band radar imagery at a frequency of 5.5405 GHz, while Sentinel-2 provides multispectral optical data across 13 spectral bands. The dataset spans the period from January 1, 2017 to March 1, 2024, and was retrieved using Google Earth Engine based on randomly sampled geographic coordinates. The study area covers tropical regions between latitudes 40°S and 40°N, within the WGS84 coordinate system.

2.2. Size of the area and data resolution

In the context of this study, the data image covering a scene of 0.1° × 0.1° (approximately 11 km × 11 km at the equator) was retrieved. All images were clipped to 512 × 512 pixels. The dataset consists of 2200 different geographic locations with corresponding images in each of the four data types described. The resolution of the data obtained from Sentinel-1 for SAR images was 10m × 10m resolution (Level-1 Ground Range Detected format) and from Sentinel-2 for optical imagery varied by band (10m, 20m, and 60m), but the RGB bands used (B2, B3, B4) which had 10m resolution.

Finally, all images were processed and stored as GeoTIFF files to preserve the geographic information, as shown in Fig. 1A and Fig. 1B, respectively. The SAR images were subjected to radiometric calibration and terrain correction (orthorectification). Optical images were filtered to ensure minimal cloud interference (less than 5% cloud cover).

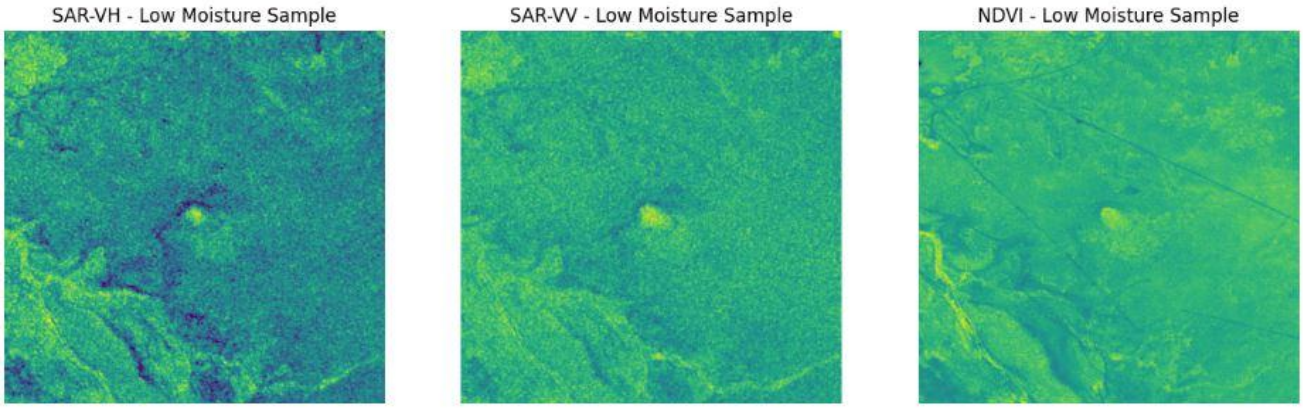

Fig. 1A. SAR and NDVI Low moisture satellite image datasets used for features extraction

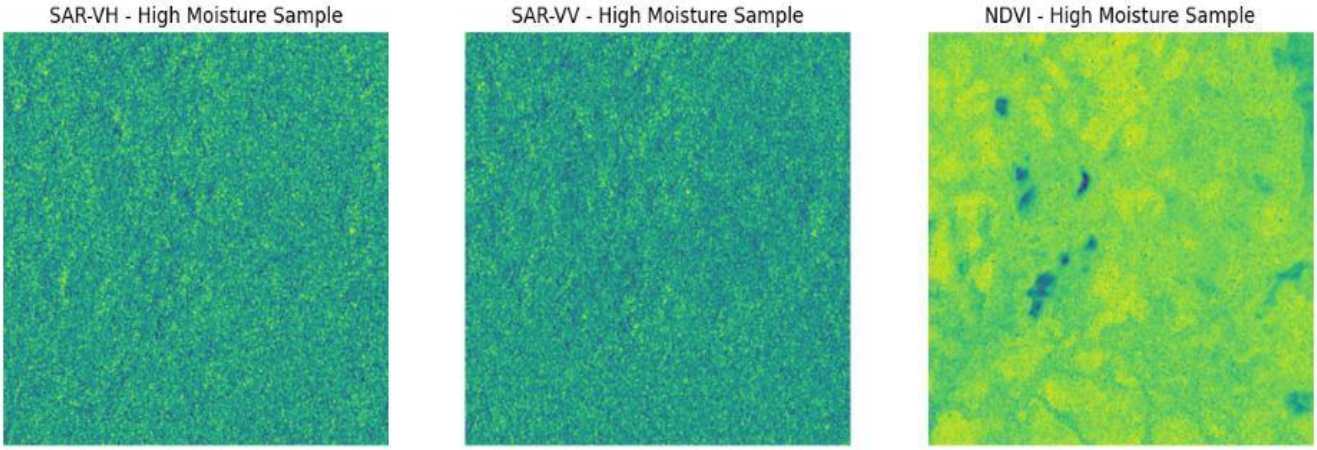

Fig. 1B. SAR and NDVI High moisture satellite image datasets used for feature extraction

The labels (ground truth) were derived from an accompanying Data.xlsx file (Diaz et al., 2024), which includes automatically computed metadata such as vegetation percentage, cloud cover, and water presence. These values were extracted using remote sensing techniques and serve as quantitative annotations for supervised learning without the need for manual labeling.

2.3. Design of deep learning surface soil moisture prediction model algorithm

The model was developed by applying multi-sensor data fusion and combining three complementary remote sensing data sources: NDVI (vegetation index), SAR VH and SAR VV polarization backscatter imagery (Fig. 2). Each data source is pre-processed by min-max normalization to standardize values between 0-1 (Equation 1).

$$I_{norm} = \frac{I - \min(I)}{\max(I) - \min(I)} \quad (1)$$

The normalized images are stacked to create a unified 3-channel feature representation that captures vegetation characteristics (NDVI) and soil surface characteristics (SAR backscatter). A composite feature set was created by stacking the normalized SAR-VH, SAR-VV, and NDVI bands. The resulting input tensor has dimensions [3, H, W], where H and W represent the spatial dimensions of the satellite imagery. It was possible to stack NDVI and SAR because they are both georeferenced and orthorectified to the same spatial framework (WGS84) and have similar ground resolutions (~10 meters). The Sentinel-1 and Sentinel-2 missions are designed to support data interoperability, allowing multi-sensor analysis without the need for additional geometric corrections (Heckel et al., 2020). In addition, all imagery was accessed through Google Earth Engine, which ensures consistent spatial alignment and projection handling.

For our target variable, we used a proxy for soil moisture derived from water and vegetation percentage measurements using Equation 2.

$$Target = \frac{Water\ Pacentage\ Mean + Vegetation\ Percentage\ Mean}{2} \quad (2)$$

This approach allows us to use available metadata as a reasonable approximation of soil moisture content. The whole fusion approach (Fig. 2) exploits the complementary nature of optical and microwave remote sensing data to improve soil moisture estimation.

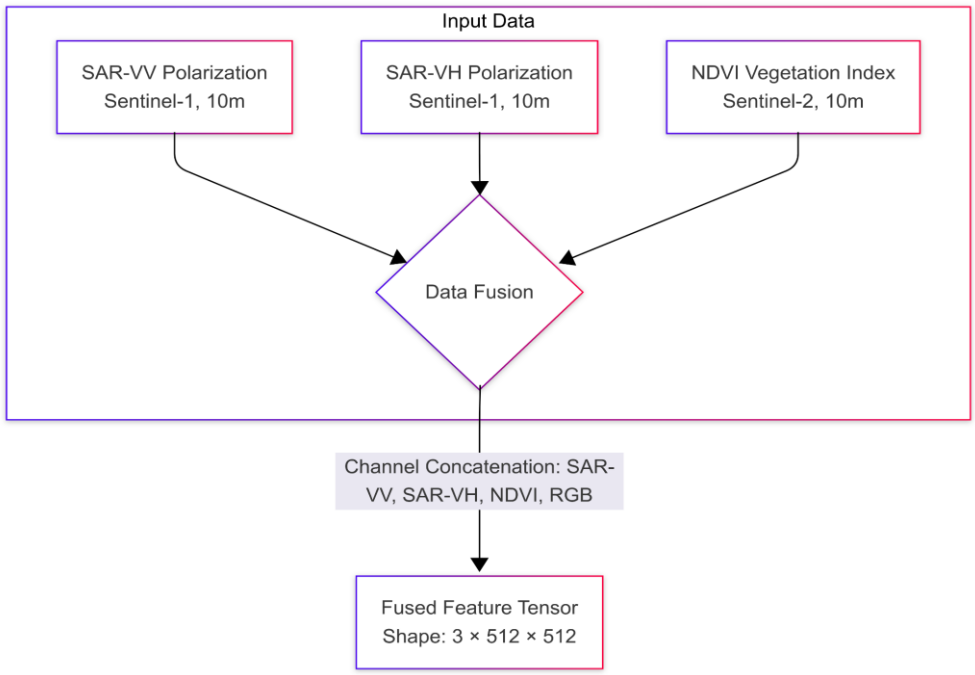

Fig. 2. Data Fusion architecture for the designed model

In designing our model, we also incorporated the residual learning technique, in which tthe core building block of our architecture is the residual blocks. Residual blocks address the challenges of training deep networks by introducing shortcut connections that bypass convolutional layers, which could help in training deep neural networks by mitigating the vanishing gradient problem. It introduces shortcut connections that bypass one or more layers, allowing the model to learn identity mappings where necessary. The structure of the residual function is given by Equation 3 below:

$$Y = F(X) + X \quad (3)$$

where $F(X)$represents the convolution operations, and (X) is the input. The network optimizes training efficiency and improves gradient flow by learning residual functions instead of direct mappings. Our model architecture consists of residual blocks that include

1. A 3×3 convolutional layer followed by batch normalization and ReLU activation
2. Another 3×3 convolutional layer followed by batch normalization
3. A shortcut connection (identity mapping or 1×1 convolution when dimensions change)
4. ReLU activation is applied to the sum of the convolution output and shortcut connection

Mathematically, the operations in a remaining block can be expressed as equations 4 and 5:

$$F(X) = W_2.\delta\big(BN(W_1.X)\big) + b_2 \quad (4)$$

$$Y = \delta.(F(X) + X) \quad (5)$$

where W_1 and W_2 are the weights of the first and second convolutional layers, respectively, b2 is the bias term, BN denotes batch normalization, and δ is the ReLU activation function. When the dimensions of $F(X)$

and X differ (e.g., when changing the number of channels), a linear projection W is applied to the shortcut connection:

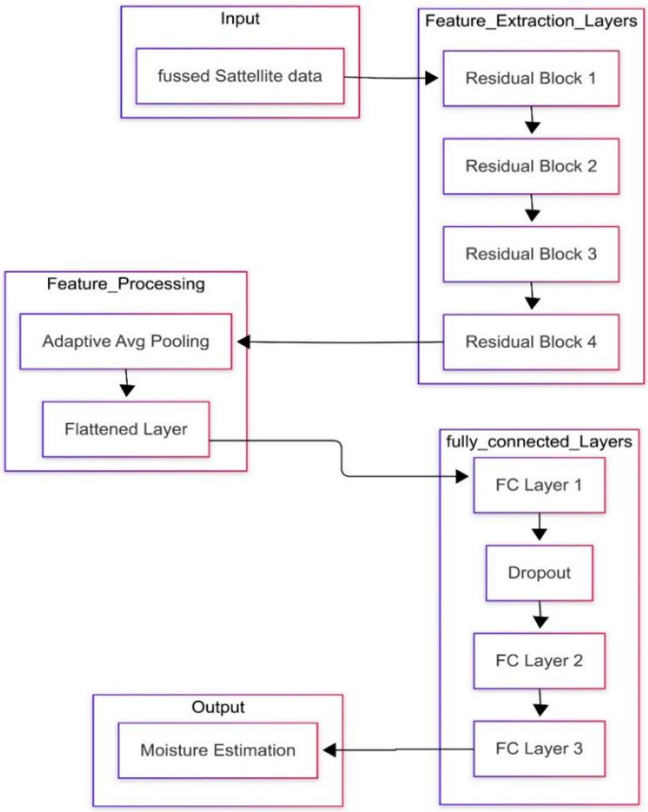

Fig. 3. An architecture of deep learning model for surface soil moisture algorithm with feature fusion and residual learning blocks

By dynamically adjusting the feature map activations, automatically fusing the channel-wise spatial information and inter-channel dependencies, and incorporating the data fusion mechanism together with the feature extraction, the model was expected to improve the accuracy and address the spatial viability to the satellite datasets in predicting the moisture of an area. Fig. 3 illustrates the overall architecture of the final designed model.

The complete designed model is generally composed of two stacked remaining blocks. The first block has input channels → 32 filters and the second block has input channels → 64 filters: 32 → 64 filters. It has global adaptive mean pooling to reduce spatial dimensions to 1×1. The fully connected layers for regression with 64 → 32 neurons and ReLU activation whose dropout (rate = 0.5). Finally, the 32 → 1 neuron is our final output.

The model takes a multi-channel satellite image as input and outputs a single value representing the estimated soil moisture. The adaptive pooling layer ensures that the model can handle input images of different spatial dimensions without requiring resizing.

2.4. Model alternatives and training procedure

We evaluated three model alternatives with identical training parameters of learning rate: 0.001, batch size: 20, and epochs: 25. First we analyzed how the designed model will behave with Simplified normal CNN architecture without feature fusion mechanisms with NDVI dataset as input, and without residual learning, the model is referred as (no_fusion model). The second alternative is the model with set up comprising with data fusion but no residual blocks or residual connections, the model is referred as (no_residual_model). Finally, the complete architecture with feature fusion and residual connections, the model is referred as (with_residual).

With each alternative, the model is trained, we evaluated the model using key three metrics which included Root Mean Squared Error (RMSE), Mean Absolute Error (MAE) and Coefficient of Determination (R^2). Table

1 below compares our model performance under described metrics. The model was trained using the Root Mean Squared Error (RMSE) loss function as shown in Equation 6:

$$L_{RMSE} = \sqrt{\frac{1}{n}\sum_{i=1}^{n}(y_i - \hat{y}_i)^2} \quad (6)$$

Where y_1 represents the true soil moisture value and $\tilde{y}_1$ is the model's prediction. Optimization is performed using the Adam optimizer with a learning rate of 0.001. Dropout regularization was employed to prevent overfitting with a rate of 0.5 before the final output layer. We also implement early stopping based on validation loss to avoid overfitting. The dataset is split into training (70%), validation (15%), and test (15%) sets. During training, multiple evaluation metrics, including RMSE, MAE and R^2 were monitored to comprehensively assess model performance as mentioned earlier.

3. RESULTS AND DISCUSSION

Tab. 1. Performance comparison of model varieties under different metrics

Variant setup	RMSE(m^3/m^3) ↓	MAE(m^3/m^3) ↓	R^2 ↑
no_fusion model	0.0296 (2.96%)	0.0318 (3.18%)	0.6839
no_residual_model	0.0205 (2.05%)	0.0293 (2.93%)	0.7139
with_residual model	0.0117 (1.17%)	0.0148 (1.48%)	0.814

The results showed that the model with feature fusion and residual learning performed better than other model variants (comparison between no_fusion model, no_residual_model and with_residual model). With similar resources such as the same type of dataset from similar sources such as Sentinel-1/2, the model achieved better metric values, for example, we obtained a lower RMSE of 0.0215 as shown in Table 1. The lower RMSE indicates good agreement between the estimated data and the observed data (Batchu, 2022). Similarly, the model that integrated feature fusion with the intentional omission of residual learning also performed better and surpassed the results of the model without feature fusion or residual learning, suggesting that feature fusion and residual learning are important for improving model performance. RMSE measures the variation between the predicted values of a model and the measured values. An observation has also revealed that: our model with feature fusion and residual learning has also yielded a better coefficient of determination (R2 =0.8139). Normally, the larger the value of R2, it means that the fitted regression equation accounts for all the variability of the values of the dependent variable in the sample data. However, in some circumstances, one can obtain a higher probability of R2 by simply fitting a regression equation that contains as many (statistically estimable) terms as there are observations (i.e., data points) (Rasheed et al., 2022). There were also better and positive results for the Mean Absolute Error (MAE), indicating that the designed model had improved performance, as shown visually in Figures 4, 5, and 6 and in Table 1.

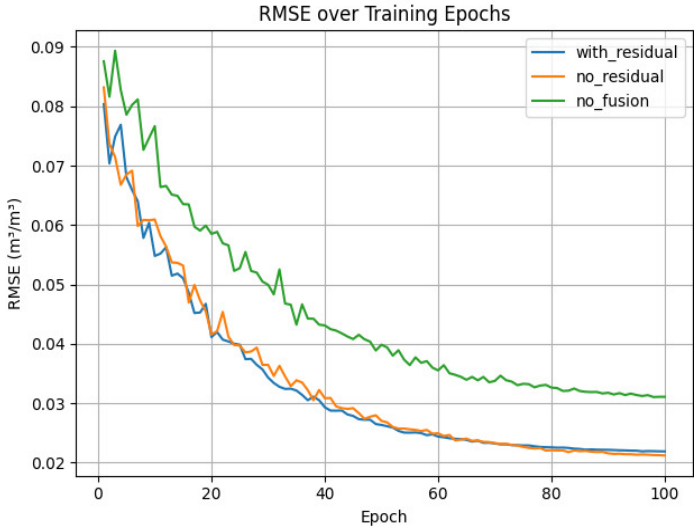

Fig. 4. RMSE performance of variants (models) over training epoch

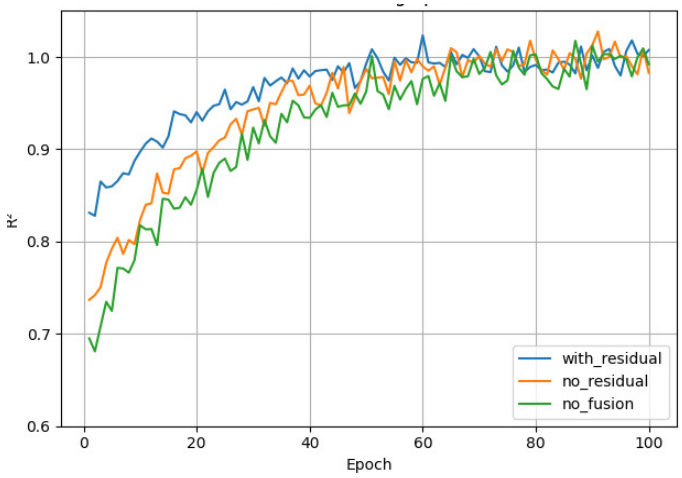

Fig. 5. Coefficient of determination (R^2) performance of variants (models) over training epoch

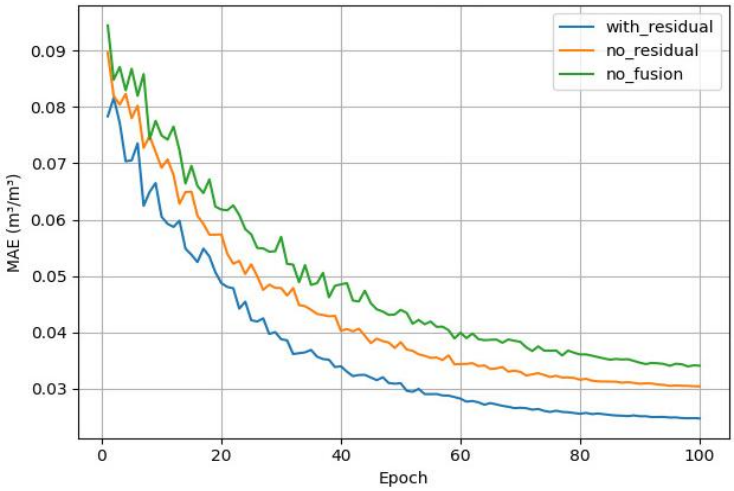

Fig. 6. Mean Absolute Error (MAE) performance of variants (models) over training epoch

4. MODAL VALIDATION

We conducted a comparison with baseline models, we compared our proposed model against single-modality approaches and traditional regression techniques such as the one used Random Forest (Rodriguez-Alvarez et al., 2023). A comparison was also made between the models using techniques such as UNet-3D and many others, as shown in Table 2. In this case, we also used the key metrics including Root Mean Squared Error (RMSE), Mean Absolute Error (MAE), and Coefficient of Determination (R^2) to compare the baseline model and our designed model. The designed model significantly outperformed the majority of baseline models, highlighting the advantage of integrating data (data fusion) and applying techniques such as feature fusion and residual learning. With our designed model using similar satellite datasets, we achieved RMSE of 0.0215 , which is typically smaller than many models outlined in our baseline comparison, its implication means with our proposed model one is assured with better performance in moisture determination.

Tab. 2. Comparison between our proposed Model and Baseline Frameworks under same Metrics same type of datasets

Rank	Model Algorithm	Dataset (Soils)	MAE (m^3/m^3)	RMSE (m^3/m^3)	R^2	Reference (DOI)
1	CatBoost (boosted trees) (Li & Yan, 2024)	In-situ 5 cm SM + Sentinel-1/2 (ShanDian Basin, China)	0.021	0.027	0.843	10.3390/land13081331
2	Random Forest (Li & Yan, 2024)	In-situ 5 cm SM + Sentinel-1/2 (ShanDian Basin, China)	0.021	0.027	0.839	10.3390/land13081331
3	Our Final designed Model (with_residual)	Sentiinel 1/2	0.0215	0.0241	0.8139	N/A
4	Convolutional Neural Network (1D-CNN) (Li & Yan, 2024)	In-situ 5 cm SM + Sentinel-1/2 (ShanDian Basin, China)	0.022	0.031	0.783	10.3390/land13081331
5	Gated Recurrent Unit (GRU)	In-situ 5 cm SM + Sentinel-1/2 (ShanDian Basin, China)	0.022	0.03	0.799	10.3390/land13081331
6	Deep Neural Network (DNN) (Li & Yan, 2024)	In-situ 5 cm SM + Sentinel-1/2 (ShanDian Basin, China)	0.023	0.032	0.765	10.3390/land13081331
7	Random Forest - Soybean field (Dinesh et al., 2024)	Simulated NISAR L-band (crop-field dataset)	0.04	0.05	0.89	10.3390/rs16183539
8	Random Forest - UAV hyperspectral (Shokati et al., 2024)	UAV hyperspectral data (agricultural site)	1.93	2.6	0.87	10.3390/rs16111962
9	Decision Tree - Corn field (Dinesh et al., 2024)	Simulated NISAR L-band (crop-field dataset)	2.42	3.1	0.3	10.3390/rs16183539
10	Random Forest - Landsat-8/9 (Shokati et al., 2024)	Landsat-8/9 satellite data (agricultural site)	2.42	4.61	0.66	10.3390/rs16111962
11	Linear Regression (Uthayakumar et al., 2022)	Wideband radar soil-moisture dataset (Singapore, 16 samples)	3.54	3.94	0.93	10.3390/s22155810
12	Random Forest - Sentinel-2 (Shokati et al., 2024)	Sentinel-2 satellite data (agricultural site)	3.43	5.95	0.49	10.3390/rs16111962
13	Decision Tree Soybean field (Dinesh et al., 2024)	Simulated NISAR L-band (crop-field dataset)	6.05	8.16	0.84	10.3390/rs16183539
14	K-Nearest Neighbors (KNN) (Uthayakumar et al., 2022)	Wideband radar soil-moisture dataset (Singapore, 16 samples)	9.27	11.51	0.41	10.3390/s22155810
15	Support Vector Machine (SVM) (Uthayakumar et al., 2022)	Wideband radar soil-moisture dataset (Singapore, 16 samples)	12.74	15.2	-0.02	10.3390/s22155810

A comparative analysis was performed using several benchmark models to evaluate the performance of the proposed model (with_residual) over different soil types. The results, presented in Table 3, show that the

proposed model consistently outperforms the benchmarks with lower Root Mean Square Error (RMSE) values, indicating improved prediction accuracy.

Tab. 3. Comparison between our proposed model and baseline frameworks between variety of soil

Study / Model Type	Sandy Soil RMSE (m^3/m^3)	Clay Soil RMSE (m^3/m^3)	Vegetated RMSE (m^3/m^3)	Bare Soil RMSE (m^3/m^3)
Our Model (with_residual)	0.0194	0.0247	0.0183	0.0258
Cai et al. (2022) ML (LightGBM)	0.024	0.037	–	–
Shi et al. (2024) Deep Learning (LSTM)	0.027	0.036	–	–
Stefan et al. (2021) SMAP + Exp. Filter	–	–	0.04	0.045
Dirmeyer et al. (2016) LSMs (NOAH-MP, CLM, etc.)	0.025	0.04	–	–
Babaeian et al. (2019) SMAP Filtered (coarse soils)	0.038	–	–	–

5. CONCLUSIONS

This study presents a novel multimodal remote sensing model with an algorithm for accurate soil moisture prediction by integrating Normalized Difference Water Index (NDWI), Synthetic Aperture Radar (SAR), and RGB satellite data sets. Through extensive validation by comparison with baseline models, the proposed approach demonstrated significantly improved performance in terms of accuracy, spatial consistency and temporal responsiveness. The model has achieved better performance metrics in terms of Root Mean Squared Error (RMSE), Mean Absolute Error (MAE), and Coefficient of Determination (R^2).

In general, the comparative analysis conducted with the baseline model has proven the potential of multimodal, data fusional, with residual learning remote sensing as a powerful tool for large-scale, real-time soil moisture monitoring. This approach has significant implications for agriculture, hydrology, and climate modeling applications, providing a scalable solution for regions with sparse soil measurements. We suggest that future areas of focus for similar work could focus more on developing models that include more components, work closer to real-time applications, and incorporate additional data sources such as weather forecasts and land surface temperature.

Conflicts of Interest

The authors declare no conflict of interest.

REFERENCES

Adab, H., Morbidelli, R., Saltalippi, C., Moradian, M., & Ghalhari, G. A. F. (2020). Machine learning to estimate surface soil moisture from remote sensing data. *Water*, *12*(11), 3223. https://doi.org/10.3390/W12113223

Babaeian, E., Sadeghi, M., Jones, S. B., Montzka, C., Vereecken, H., & Tuller, M. (2019). Ground, proximal, and satellite remote sensing of soil moisture. *Reviews of Geophysics*, *57*(2), 530–616. https://doi.org/10.1029/2018RG000618

Batchu, V. (2022). A machine learning data fusion model for soil moisture retrieval. *ArXiv, abs/*2206.09649. https://doi.org/10.48550/arXiv.2206.09649

Brocca, L., Melone, F., Moramarco, T., & Morbidelli, R. (2010). Spatial-temporal variability of soil moisture and its estimation across scales. *Water Resources Research*, *46*(2). https://doi.org/10.1029/2009WR008016

Diaz, J., Vasquez, R., Garavito-Gonzalez, A. F., & Vásquez, E. (2024). *Dataset of Sentinel-1 SAR and Sentinel-2 NDVI imagery* (Version 3) [Data set]. Mendeley Data. https://doi.org/10.17632/xjcr5k4c9t.3

Dinesh, D., Kumar, S., & Saran, S. (2024). Machine learning modelling for soil moisture retrieval from simulated NASA-ISRO SAR (NISAR) L-Band Data. *Remote Sensing*, *16*(18), 3539. https://doi.org/10.3390/RS16183539

Famiglietti, J. S., Ryu, D., Berg, A. A., Rodell, M., & Jackson, T. J. (2008). Field observations of soil moisture variability across scales. *Water Resources Research*, *44*(1), W01423. https://doi.org/10.1029/2006WR005804

Heckel, K., Urban, M., Schratz, P., Mahecha, M. D., & Schmullius, C. (2020). Predicting forest cover in distinct ecosystems: The potential of multi-ssource Sentinel-1 and -2 data fusion. *Remote Sensing*, *12*(2), 302. https://doi.org/10.3390/RS12020302

Hunduma, S., & Kebede, G. (2020). Indirect methods of measuring soil moisture content using different Sensors 1. *African Journal of Basic & Applied Sciences*, *12*(3), 37–55. https://doi.org/10.5829/idosi.ajbas.2020.37.55

Li, M., & Yan, Y. (2024). Comparative analysis of machine-learning models for soil moisture estimation using high-resolution remote-sensing data. *Land*, *13*(8), 1331. https://doi.org/10.3390/LAND13081331

Massari, C., Su, C. H., Brocca, L., Sang, Y. F., Ciabatta, L., Ryu, D., & Wagner, W. (2017). Near real time de-noising of satellite-based soil moisture retrievals: An intercomparison among three different techniques. *Remote Sensing of Environment*, *198*, 17–

29. https://doi.org/10.1016/J.RSE.2017.05.037
Mohanty, B. P., & Skaggs, T. H. (2001). Spatio-temporal evolution and time-stable characteristics of soil moisture within remote sensing footprints with varying soil, slope, and vegetation. *Advances in Water Resources*, *24*(9–10), 1051–1067. https://doi.org/10.1016/S0309-1708(01)00034-3
Rasheed, M. W., Tang, J., Sarwar, A., Shah, S., Saddique, N., Khan, M. U., Imran Khan, M., Nawaz, S., Shamshiri, R. R., Aziz, M., & Sultan, M. (2022). Soil moisture measuring techniques and factors affecting the moisture dynamics: A comprehensive review. *Sustainability*, *14*(18), 11538. https://doi.org/10.3390/su141811538
Rodriguez-Alvarez, N., Munoz-Martin, J. F., & Morris, M. (2023). Latest advances in the global navigation satellite system - reflectometry (GNSS-R) field. *Remote Sensing*, *15*(8), 2157. https://doi.org/10.3390/RS15082157
Scott, C. A., Bastiaanssen, W. G. M., & Ahmad, M.-D. (2003). Mapping root zone soil moisture using remotely sensed optical imagery. *Journal of Irrigation and Drainage Engineering*, *129*(5), 326–335. https://doi.org/10.1061/(ASCE)0733-9437(2003)129:5(326)
Shokati, H., Mashal, M., Noroozi, A., Abkar, A. A., Mirzaei, S., Mohammadi-Doqozloo, Z., Taghizadeh-Mehrjardi, R., Khosravani, P., Nabiollahi, K., & Scholten, T. (2024). Random forest-based soil moisture estimation using Sentinel-2, Landsat-8/9, and UAV-Based hyperspectral data. *Remote Sensing*, *16*(11), 1962. https://doi.org/10.3390/rs16111962
Uthayakumar, A., Mohan, M. P., Khoo, E. H., Jimeno, J., Siyal, M. Y., & Karim, M. F. (2022). Machine learning models for enhanced estimation of soil moisture using wideband radar sensor. *Sensors*, *22*(15), 5810. https://doi.org/10.3390/S22155810